IEEE Access
Multidisciplinary | Rapid Review | Open Access Journal

IEEE POWER & ENERGY SOCIETY SECTION

Received November 7, 2020, accepted November 25, 2020, date of publication December 7, 2020,
date of current version December 18, 2020.

Digital Object Identifier 10.1109/ACCESS.2020.3042784

Online Assessment of Transient Stability of Grid Connected PV Generator With DC Link Voltage and Reactive Power Control

INDLA RAJITHA SAI PRIYAMVADA, (Graduate Student Member, IEEE), AND SARASIJ DAS, (Senior Member, IEEE)
Indian Institute of Science, Bengaluru 560012, India

Corresponding author: Sarasij Das (sarasij@iisc.ac.in)

This work was supported by the Prime Minister's Research Fellows Grant, Government of India.

ABSTRACT The proliferation of Photovoltaic (PV) generation has brought several changes in the transient stability analysis of power systems. The rotor angle dynamics based stability analysis used for synchronous generators may not be applicable for PV generators. In the existing literature, the transient stability of a grid connected PV generator with dc link voltage and reactive power control (V_{dc} and Q control) is analyzed from the coupled nonlinear functions corresponding to PV control loops, Phase Locked Loop (PLL) and network dynamics. The existing method may not be suitable for online transient stability assessment because it is computationally heavy. This paper proposes an online transient stability criterion for a PV generator (with V_{dc} and Q control) connected to grid modelled as infinite bus. The PV generator is considered to have Low Voltage Ride Through (LVRT) capability, but does not provide voltage support. In this study, the relation between the ac and dc side dynamics is explored. A stability criterion is proposed to assess the transient stability by monitoring the swing in the energy of the dc link capacitor. The proposed criterion requires the dc link voltage trajectory only till the first swing of the dc link voltage. As a result, the proposed assessment criterion is computationally less demanding and less prone to measurement errors in comparison to existing methods. Thus, the proposed criterion is suitable for online transient stability assessment. The effectiveness of the proposed criterion is verified for single-stage as well as two-stage converter configurations of PV generator. The proposed criterion is also verified on a modified IEEE 39 bus system. Time-domain simulations are carried out to validate the proposed criterion. The proposed approach is compared with an existing transient stability criterion for V_{dc} and Q control based grid connected PV generator. The advantages of the proposed method as compared to the existing method are discussed.

INDEX TERMS Transient stability, photovoltaic generation, power system dynamics, inverter interfaced generation, stability assessment.

I. INTRODUCTION

In transition towards green energy, the penetration of Photo Voltaic (PV) generators is increasing in power system. Power electronic converters are used for interfacing the PV generations with grid to enable proper control and operation. In conventional power system, transient stability is assessed using the swing equation of the Synchronous Generator (SG) rotor angle and equal area criterion [1]. However, the dynamic response of the PV generators is mainly dictated by their control structure [2]. The conventional equal area criterion may not be valid for transient stability assessment of PV generators. In addition, the converters of PV generators provide flexibility to alter the PV control strategy online so as to adapt to the power system changes. This flexibility helps in improving the transient stability of grid connected PV generators by designing corrective actions. However, online transient stability assessment is required in order to trigger the corrective actions in case of a contingency. So, there is a need to develop online analysis methods to assess the transient stability of PV generations which has potential to improve the grid reliability.

The stability of grid-connected converter interfaced generators is discussed in some of the recent works. The study

The associate editor coordinating the review of this manuscript and approving it for publication was Guangya Yang.

carried out in [3] discusses transient stability of Power Synchronization Control (PSC) based converter interfaced generator using phase portraits. However, [3] does not consider the inner control loops dynamics in the stability analysis. The work presented in [4] analyzes the stability of Inverter Interfaced Distributed Generations (IIDG) with virtual SG control using Lyapunov functions. The work carried out in [5] presents a stability criterion for grid connected PV generator with real power and reactive power (PQ) control using nonlinear functions formulated from control equations. The stability of virtual SG control based IIDG is analyzed in [6] considering the current limits of inverters. A stability criterion for grid connected PV generator with PQ control using energy functions is presented in [7]. The risk of Loss of Synchronism (LOS) of Inverter Interfaced Generator (IIG) is analyzed in [8]–[10] considering a reduced order non-linear model of PLL. The LOS of Voltage Source Converters (VSC) under weak grid conditions is discussed in [11]. However, the dynamics of the current control loops are not discussed in the works [8]–[11]. The transient stability of different grid-forming control based VSC is presented in [12] considering first and second order control loops. The virtual power angle of VSC is investigated in [13] to carry out the transient stability analysis of droop control based VSC. The transient stability of grid connected PV generator with dc link control is analyzed in [14] by investigating the PV control loops. The stability analysis of IIDGs with induction machine loads is presented in [15] through eigen-value analysis. The stability analysis of IIG using impedance modelling is carried out in [16]. The instability of PV generator considering the non-linearity in the power reference is analyzed in [17] through the Nyquist analysis. The limitations of the existing literature are summarized as:

- The transient stability of VSC is explored well from the synchronization stability perspective. However, the impact of current control dynamics on stability of grid connected VSC is not investigated well in the literature.
- The transient stability analysis considering the combined effect of the inner and outer PV control loops (with current and duty ratio saturation), PLL dynamics and dc link capacitor dynamics is not well explored.
- The dc link voltage control is identified to be commonly used control for PV generators [18]. However, there is limited literature on transient stability analysis of dc link voltage (V_{dc}) and reactive power (Q) control based PV.
- The transient stability analysis of V_{dc} and Q control based PV is presented in [14]. Literature [14] requires computation of the area under the two non-linear functions to assess the PV generator stability. Even though the transient stability assessment method presented in [14] gives a comprehensive insight on ac side dynamics, this approach is computationally heavy and will be difficult to implement online.

So, there is need for a computationally efficient criterion for online transient stability assessment of V_{dc} and Q control based PV generators. This paper tries to fill the gap.

Single Machine Infinite Bus (SMIB) system is commonly used for analyzing the transient stability of grid connected synchronous generator. Similarly, to study the transient stability of grid connected PV generator, a Single PV Infinite Bus (SPIB) system is considered in this paper. The study carried out in this paper analyzes the transient stability of a PV generator connected to grid modelled as an infinite bus. The PV generator is controlled through V_{dc} and Q control strategy. The solar irradiance is considered to be constant (i.e. V_{dc}^{ref} is constant) during the fault duration. The PV generator is considered to have the Low Voltage Ride Through (LVRT) capability, but does not have voltage support functionality.

The main contributions of this paper are:

- A computationally efficient criterion to assess the transient stability of grid connected PV with V_{dc} and Q control is proposed.
- The coupled and nonlinear dynamic equations of the network and PV control loops make the transient stability analysis difficult to analyze theoretically. So, the coupling between ac side and dc side quantities of the PV converter is explored in this work to analyze the transient stability. Due to the coupling of ac and dc side dynamics, the combined effect of the inner and outer PV control loops, PLL and dc link capacitor dynamics will be reflected on to the dc side. The novelty of this work lies in assessing the transient stability of PV generator from dc link voltage dynamics which is computationally efficient. Analyzing transient stability of PV based on dc side dynamics is not explored in the existing literature.
- The stability criterion proposed in this paper can assess the transient stability of grid connected PV from dc link voltage dynamics alone unlike [5], [7], [14] which require dynamics of multiple ac side quantities. So, the proposed criterion has computational advantage over the methods proposed in [5], [7], [14]. The proposed criterion is less prone to measurement errors compared to existing methods. So, the proposed transient stability assessment method is efficient to implement online.

The proposed criterion is verified on two different configurations of PV viz., single stage and two stage, to check for the generality. The criterion is verified on SPIB system and a modified IEEE 39 bus benchmark system. The results obtained from the proposed criterion are validated through time-domain simulations. The comparison of the proposed criterion with a transient stability criterion available in existing literature is also presented.

The proposed criterion for transient stability can be used for detecting system instability online and triggering special protection schemes or corrective actions to restore system stability. The criterion can also be used for implementing adaptive control schemes in PV converters to enhance power system stability.

II. TRANSIENT STABILITY OF SPIB SYSTEM

A. SINGLE PV GENERATOR- INFINITE BUS SYSTEM

The block diagram of grid connected PV generator system is shown in Fig. 1(a). The grid is modelled as an infinite bus in this study. A stability criterion is developed by analyzing the dynamics of SPIB system as shown in Fig. 1(b). The network transients of the system are also considered during the stability analysis. The VSC based PV generator is controlled through dc link voltage (V_{dc}) and reactive power (Q) control strategy as shown in Fig. 2 [18]. The reference to the dc voltage control loop of Fig. 2 is generated through Maximum Power Point Tracking (MPPT) technique. The control strategy does not include the grid support functions. The voltage magnitude and phase angle at the PV generator terminals are controlled indirectly by the PV controls [19]. It is achieved by controlling the voltage at the terminals of dc-ac converter through the modulation signals d_d and d_q as shown in Fig. 1(b). The space vector reference (or dq) frame generated by the PLL is used for the PV generator control. The real (or d) axis of reference (or dq) frame generated by PLL is aligned with PV terminal voltage phasor i.e. $V_{pv} = |V_{pv_d}| + j0$ in dq frame. It is to be noted that the PV generator has the LVRT capability thereby it remains connected to the grid during fault. In this work the stability assessment is done considering faults on the transmission line connecting PV to the grid. The solar irradiance is considered to be constant (i.e. V_{dc}^{ref} is constant) during the fault duration.

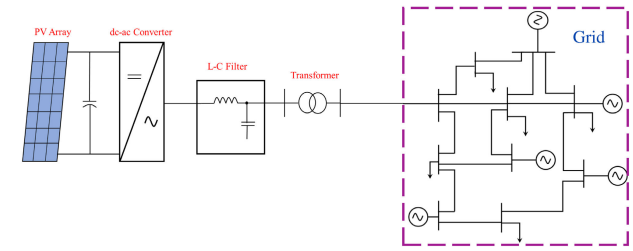

(a) Block diagram of grid connected PV generator system

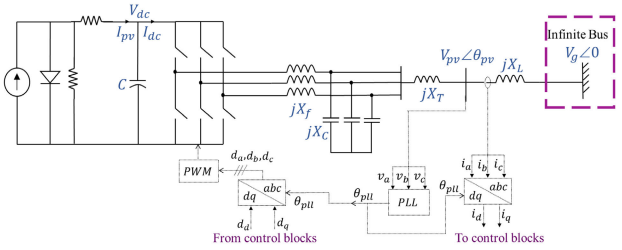

(b) Single PV Infinite Bus (SPIB) model

FIGURE 1. Grid connected PV generator system.

B. TRANSIENT STABILITY DEFINITION FOR SPIB SYSTEM

The transient stability of power systems is defined as the ability of the system to regain an operating equilibrium after being subjected to a large disturbance like faults on transmission lines or loss of a large generator [20]. In SG dominated power systems, the large disturbances can lead to angle and voltage instability. If the large disturbance leads to tripping of a generator or formation of islands, it may lead to frequency instability. This classification of stability is done based on the system variable in which instability can be observed [20]. This distinction is possible in the conventional power systems because of the difference in the response times (time constant) of system variables.

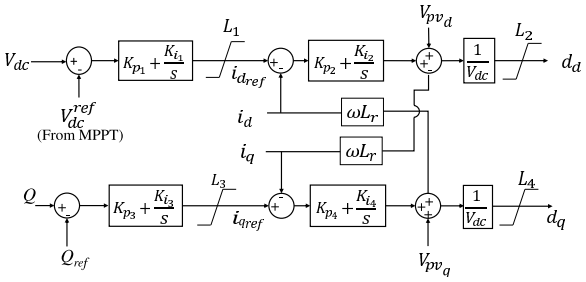

FIGURE 2. Control loops of PV generator.

However, in the SPIB system, the dynamics of all the system state variables are mostly dictated by the PV control and PLL dynamics [2]. This is due to the fact that the rest of the grid is considered to be a stiff source with constant voltage and frequency. Any disturbance on the SPIB system will appear as a disturbance to both the PV control loops, V_{dc} and Q control and PLL. So, the SPIB system is said to be transient stable if the PLL and PV converter controls are able to reach steady state (i.e. stability of controls), even after the system is subjected to a large disturbance.

III. PROPOSED METHOD TO ASSESS TRANSIENT STABILITY OF SPIB SYSTEM

In section II, it is identified that the transient stability of SPIB system is dictated by the stability of PV generator controls (i.e converter controls and PLL stability). In this section, a method to assess transient stability of SPIB system is proposed by exploring the relation between converter control loops, PLL stability and dc link capacitor dynamics. Firstly, the complexity involved in analyzing the transient stability using converter control loops and PLL dynamics is discussed. Secondly, the relation between the ac side control loop dynamics and dc link voltage dynamics of PV is presented. Thirdly, a criterion is proposed to assess the transient stability by analyzing the dc link capacitor voltage dynamics.

A. COUPLING BETWEEN AC-SIDE CONVERTER CONTROL, PLL DYNAMICS AND DC LINK CAPACITOR DYNAMICS

In case of a disturbance, the PLL tries to trace the voltage phase angle at the PV generator terminals. This helps the PV generator to remain in synchronism with rest of the grid. The block diagram of a basic Synchronous Reference Frame PLL is represented in Fig. 3. Using the block diagram of PLL and the expression $v_q = V_{pv}\ \sin(\theta_{pv} - \theta_{pll})$ [21]:

$$\theta_{pll} = \int \omega_{nom}\, dt + \int \left(K_p V_{pv} \sin(\theta_{pv} - \theta_{pll}) + K_i \int V_{pv} \sin(\theta_{pv} - \theta_{pll}) \right) dt$$

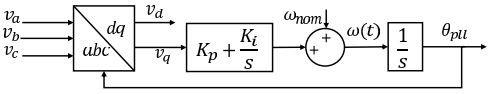

FIGURE 3. Block diagram of Synchronous Reference Frame PLL.

$$\begin{aligned}\implies & \frac{d^2\theta_{pll}}{dt^2} + K_p V_{pv}\cos(\theta_{pv}-\theta_{pll})\frac{d\theta_{pll}}{dt} \\ = \; & K_i V_{pv}\sin(\theta_{pv}-\theta_{pll}) + K_p V_{pv}\cos(\theta_{pv}-\theta_{pll})\frac{d\theta_{pv}}{dt} \\ & + K_p\sin(\theta_{pv}-\theta_{pll})\frac{dV_{pv}}{dt} \end{aligned} \tag{1}$$

Here, θ_{pll} tries to trace θ_{pv} so as to align d axis of PLL frame with PV terminal voltage. The dynamics of PLL are governed by (1). The dq reference traced by the PLL serves as reference frame for the converter control loops. The converter control loops determine the current injection from PV generator into the grid by controlling the voltage at the terminals of converter [19]. The relation between the current injections and the converter terminal voltage can be expressed as:

$$\begin{aligned} L_r\frac{di_d}{dt} &= d_d V_{dc} - V_{pv_d} + \omega(t) L_r i_q \\ L_r\frac{di_q}{dt} &= d_q V_{dc} - V_{pv_q} - \omega(t) L_r i_d \end{aligned} \tag{2}$$

where, $V_{pv_d} = V_{pv}\cos(\theta_{pv}-\theta_{pll})$; $V_{pv_q} = V_{pv}\sin(\theta_{pv}-\theta_{pll})$. For formulating (2), current flowing through the capacitance of LC filter is neglected. In (2), L_r is the equivalent inductance of LC filter and transformer; (i_d, i_q), (V_{pv_d}, V_{pv_q}) and $(d_d V_{dc}, d_q V_{dc})$ represent the d and q components of the current output of PV, PV terminal voltage and voltage at converter terminals respectively; $\omega(t)$ represents the frequency estimated by PLL as shown in Fig. 3. The modulation signals d_d and d_q generated by the control loops can be expressed as:

$$\begin{aligned} d_d V_{dc} &= K_{p_2}(i_{d_{ref}} - i_d) + K_{i_2}\int (i_{d_{ref}} - i_d)\,dt + V_{pv_d} - X_r i_q \\ d_q V_{dc} &= K_{p_4}(i_{q_{ref}} - i_q) + K_{i_4}\int (i_{q_{ref}} - i_q)\,dt + V_{pv_q} + X_r i_d \\ i_{d_{ref}} &= K_{p_1}(V_{dc} - V_{dc}^{ref}) + K_{i_1}\int (V_{dc} - V_{dc}^{ref})\,dt \\ i_{q_{ref}} &= K_{p_3}(Q - Q_{ref}) + K_{i_3}\int (Q - Q_{ref})\,dt \end{aligned} \tag{3}$$

The current references $i_{d_{ref}}$ and $i_{q_{ref}}$ are limited by L_1 and L_3 as shown in Fig. 2 based on the current carrying capability limit of the dc-ac converter. Similarly, the d_d and d_q signals are also limited (L_2 and L_4) based on the duty ratio limits of converter switches. In order to analyze the converter control loop and PLL stability, (1) - (3) have to be analyzed. These coupled and nonlinear differential equations make the stability assessment very difficult through analytical approaches. In addition, assessing the stability of grid connected PV generator from these coupled nonlinear equations will be computationally demanding. However, due to the coupling between the ac and dc sides of VSC, the dynamics of both the converter control loops will be reflected in the dynamics of dc link capacitor voltage. The coupling between ac and dc sides is derived in the following paragraphs.

The dynamics of dc link voltage are governed by the capacitor current-voltage relation (4). Consider the dc link capacitor dynamic equation:

$$C\frac{dV_{dc}}{dt} = I_{pv} - I_{dc} \tag{4}$$

where, I_{pv} and I_{dc} represent the PV array output current and dc side current of VSC; C represents dc link capacitance. The I_{dc} can be expressed in terms of ac side currents as:

$$I_{dc} = d_q i_q + d_d i_d \tag{5}$$

Substituting (5) in (4):

$$C\frac{dV_{dc}}{dt} = I_{pv} - (d_q i_q + d_d i_d) \tag{6}$$

Multiplying (6) with V_{dc} on both sides:

$$\begin{aligned} CV_{dc}\frac{dV_{dc}}{dt} &= V_{dc}I_{pv} - (d_q V_{dc} i_q + d_d V_{dc} i_d) \\ \implies \frac{1}{2}C\frac{dV_{dc}^2}{dt} &= V_{dc}I_{pv} - (d_q V_{dc} i_q + d_d V_{dc} i_d) \end{aligned} \tag{7}$$

Substituting (3) in (7):

$$\begin{aligned} & \frac{1}{2}C\frac{dV_{dc}^2}{dt} \\ = \; & V_{dc}I_{pv} \\ & - \Big(K_{p_4}(i_{q_{ref}} - i_q) + K_{i_4}\int (i_{q_{ref}} - i_q)\,dt + V_{pv_q} + X_r i_d\Big) i_q \\ & - \Big(K_{p_2}(i_{d_{ref}} - i_d) + K_{i_2}\int (i_{d_{ref}} - i_d)\,dt + V_{pv_d} - X_r i_q\Big) i_d \\ \implies & \frac{1}{2}C\frac{dV_{dc}^2}{dt} \\ = \; & V_{dc}I_{pv} - (V_{pv_d} i_d + V_{pv_q} i_q) \\ & - \Big(K_{p_4}(i_{q_{ref}} - i_q) + K_{i_4}\int (i_{q_{ref}} - i_q)\,dt\Big) i_q \\ & - \Big(K_{p_2}(i_{d_{ref}} - i_d) + K_{i_2}\int (i_{d_{ref}} - i_d)\,dt\Big) i_d \\ \implies & \frac{1}{2}C\frac{dV_{dc}^2}{dt} \\ = \; & V_{dc}I_{pv} - \Big(V_{pv}\cos(\theta_{pv}-\theta_{pll}) i_d + V_{pv}\sin(\theta_{pv}-\theta_{pll}) i_q\Big) \\ & - \Big(K_{p_4}(i_{q_{ref}} - i_q) + K_{i_4}\int (i_{q_{ref}} - i_q)\,dt\Big) i_q \\ & - \Big(K_{p_2}(i_{d_{ref}} - i_d) + K_{i_2}\int (i_{d_{ref}} - i_d)\,dt\Big) i_d \end{aligned} \tag{8}$$

From (8) and (3), it can be concluded that the dc link voltage dynamics are coupled with the following ac-side dynamics:

- The PV control loops are coupled through d_d and d_q terms of (7) which are expanded in (8) to reflect the PV inner and outer control loop dynamics.
- The PLL dynamics are coupled through θ_{pll} terms in (8). The dynamics of θ_{pll} are expressed in (1) for SRF-PLL. If the PLL loses its stability (i.e. LOS), then dc link voltage also becomes unstable. Hence, the instability of

PLL (LOS) can also be captured using the dc link voltage dynamics.

- The network dynamics are coupled through the V_{pv} term. As V_{dc} and Q control is a grid-following control, the terminal voltage magnitude of PV i.e. V_{pv} is dictated by the grid voltage and the transmission line connecting PV to grid.

So, it is clear that the dc link capacitor dynamics will act as an indicator for the dynamics of all the ac-side quantities. So, it can be concluded that the ac-side converter control loops and PLL stability can be analyzed from the dc-link capacitor voltage dynamics. Hence, the transient stability of the SPIB system can be assessed by analyzing the dc-link voltage dynamics alone. In this work, the transient stability is assessed using the dc link voltage dynamics because of the simplicity of this approach compared to that of ac side control loops and PLL.

B. ASSESSING TRANSIENT STABILITY OF GRID CONNECTED PV GENERATOR

In section III-A, the coupling between the ac and dc side dynamics is discussed. This section presents the criterion to assess transient stability of the grid connected PV generator using the energy stored in dc link capacitor.

The main idea behind the proposed criterion is to analyze the net energy stored in the dc link capacitor following a disturbance on the system. In case of short circuit faults, if the energy accumulated during fault is delivered back to the system after clearing the fault then the system will remain stable. The dc link voltage V_{dc} is representative of the energy stored in the dc link capacitor. So, a transient stability assessment criterion is proposed here by monitoring the V_{dc} trajectory. The detailed discussion on formulation and implementation of the proposed criterion is presented in the following paragraphs.

Due to the coupling between ac and dc sides, any disturbance on ac side of SPIB system will lead to oscillations in the dc link voltage. The stability of the system will depend on damping of these oscillations. The control structure of PV generator comprises of several control loops as shown in Fig. 2 and Fig. 3. The PV outer control loops of Fig. 2 are comparatively slower than the inner current control loops and PLL [19]. The interactions among these control loops may lead to more than one frequency component of oscillations in the dc link voltage when a disturbance is created on ac side of PV. So, due to the control structure of the PV generator, either of the following two scenarios may arise after fault clearance. The dc link voltage trajectory $V_{dc}(t)$ can have:

1) only one oscillation frequency component superimposed on dc quantity as shown in Fig. 4(a).
2) low and high frequency oscillation components superimposed on dc quantity as shown in Fig. 4(b).

It is to be noted that the categorization of low and high frequency components is made based on the relative difference between the oscillation frequency. These oscillations are due to the dc link and PV control loops of SPIB system. It should not be confused with the inter area low frequency modes of conventional power systems. The frequencies of the components of V_{dc} trajectory depend on the control loop time constants and the PV generator parameters. The low frequency oscillation corresponds to the outer control loop. The high frequencies correspond to the inner control loops, network dynamics, PLL and filter dynamics. The method to analyze the dynamics of dc link voltage for these two scenarios is discussed in the following subsections.

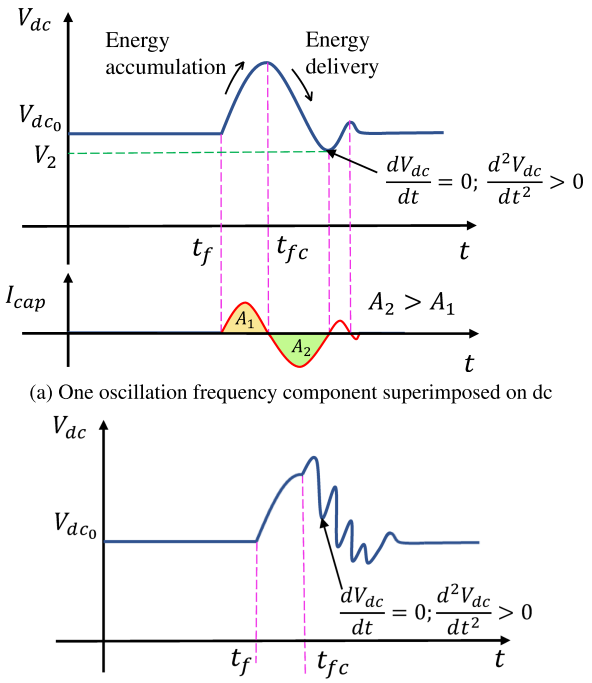

(a) One oscillation frequency component superimposed on dc

(b) Low and high frequency oscillation components superimposed on dc

FIGURE 4. Representative dynamics of dc link capacitor voltage for stable case.

1) In this scenario, the dc link voltage trajectory is a resultant of one oscillation frequency component superimposed on dc quantity. During a short circuit fault, the real power output of PV generator will be less than the power output in normal operation. So, the voltage of dc link capacitor keeps increasing during the fault due to the energy accumulation in the capacitor. The voltage keeps increasing till it reaches the PV array no-load voltage as the dc link capacitor is present across the terminals of the PV array as shown in Fig. 1(b). Once the fault is cleared, the dc link voltage starts to decrease as the energy is delivered back into the grid. Representative voltage and current dynamics of dc link capacitor in a stable scenario are shown in Fig. 4(a). As shown in Fig. 4(a), the dc link voltage will settle to a stable operating point if the energy accumulated during fault is delivered back to the system after clearing the fault. It is known that the energy stored in the capacitor is a reflection of charge accumulated in the capacitor i.e. area under the dc link capacitor current I_{cap} versus t curve as shown in Fig. 4(a). I_{cap} denotes current through the dc link and $I_{cap} = I_{pv} - I_{dc}$. For the dc link voltage

to be stable, the positive area under the current vs. time plot, A_1, should be less than or equal to the negative area, A_2. The stability can be assessed from the first swing of I_{cap}. This is due to the inherit damping of I_{cap} provided by the control loops. Due to the damping, the charge accumulated under the curve in subsequent swings will be less than that of in the first swing. The instants on the current vs. time plot can be mapped on to the voltage vs. time plot as shown in Fig. 4(a). The net energy accumulated in the dc link by the end of the first swing of the capacitor current can be observed from the voltage of the dc link at the instant when $\frac{dV_{dc}}{dt} = 0$ and $\frac{d^2V_{dc}}{dt^2} > 0$. Consider that $t = t^*$ denotes the time instant when $\frac{dV_{dc}}{dt} = 0$ and $\frac{d^2V_{dc}}{dt^2} > 0$. So, in stable operation scenario (shown in Fig. 4(a)):

$$\frac{dV_{dc}}{dt} = 0\Big|_{t=t^*} \;\&\; \frac{d^2V_{dc}}{dt^2} > 0\Big|_{t=t^*} \;\&\; V_{dc}(t^*) \leq V_{dc_0} \qquad (9)$$

where, V_{dc_0} is the pre-fault operating voltage of dc link. In the similar lines, the typical dynamics of the dc link capacitor voltage for the case when at $t = t^*$, $V_{dc}(t) = V_{dc_0}$ is presented in Fig. 5(a). The case when $V_{dc}(t^*) > V_{dc_0}$ is presented in Fig. 5(b).

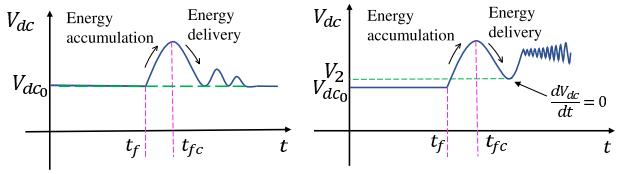

(a) Stable: $V_{dc}(t) = V_{dc_0}$ when $t = t^*$ (b) Unstable: $V_{dc}(t) > V_{dc_0}$ when $t = t^*$

FIGURE 5. Typical dynamics of dc link capacitor voltage.

2) In this scenario, the dc link voltage is resultant of low and high frequency oscillation components superimposed on dc quantity. Due to the interaction among the control loops of PV generator, it is possible that the V_{dc} trajectory after the fault clearance could consist of more than one oscillation frequency component. The Fig. 4(b) shows representative dynamics of dc link voltage which is a resultant of low and high frequency components superimposed on dc. It can be seen that the criterion (9) would result in wrong conclusions on the stability of the system, when applied on the resultant trajectory of V_{dc}. In these scenarios, online signal decomposition techniques [22]–[24] can be used to separate V_{dc} trajectory into a set of higher frequency components and a relatively low frequency component superimposed on dc as shown in Fig. 6. In Fig. 6, $V_{dc_{\{l\}}}$ denotes the lowest frequency component superimposed on dc quantity; $V_{dc_{\{i\}}}$, $i = 1, 2 \ldots n$ denotes the higher frequency components. After the decomposition, $t = t^*$ instant (where, $\frac{dV_{dc}}{dt} = 0$ & $\frac{d^2V_{dc}}{dt^2} > 0$) is calculated for the lowest frequency component of the trajectory. For the SPIB system to be stable, the $t = t^*$ instant (after fault clearance) in the lowest frequency component should occur when $V_{dc}(t^*) \leq V_{dc_0}$.

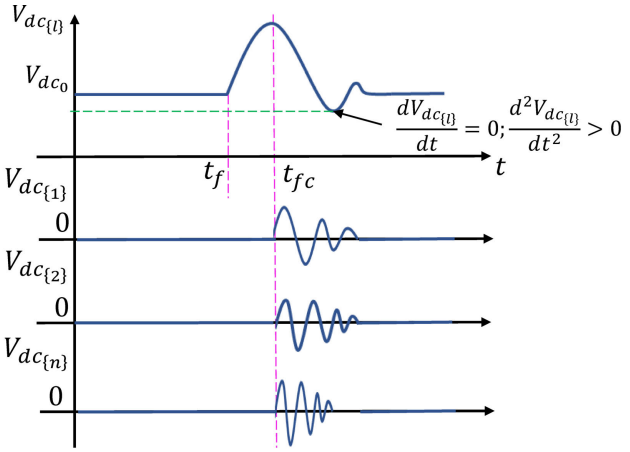

FIGURE 6. Dynamics of dc link capacitor voltage after signal decomposition.

In addition, the components $V_{dc_{\{i\}}}$, $i = 1, 2 \ldots n$ should have positive damping for the system to be stable. The magnitude of consecutive peaks of these components can be analyzed to check for positive damping. The damping coefficient of $V_{dc_{\{i\}}}$ can be estimated before the $t = t^*$ instant as these components have higher frequency as compared to that of $V_{dc_{\{l\}}}$. On the other hand, the estimation of the damping of oscillations in $V_{dc_{\{l\}}}$ by investigating its peaks would require V_{dc} trajectory for longer duration than the first swing (thereby increasing the computational burden). So, it is efficient to estimate the damping of oscillations in $V_{dc_{\{l\}}}$ by investigating $V_{dc}(t)$ value at $t = t^*$ instant.

C. SUMMARY OF THE PROPOSED CRITERION

The proposed stability criterion can be summarised as:

- The SPIB system is stable if condition (9) is satisfied after the fault clearance. In terms of net area under current vs. time plot, the criterion can be expressed as $(A_1 - A_2) \leq 0$ in the first swing of current through dc link capacitor, as shown in Fig. 4.
- The SPIB system is unstable if after the fault clearance, $V_{dc}(t^*) > V_{dc_0}$ where, $t = t^*$ denotes the time instant when $\frac{dV_{dc}}{dt} = 0$ and $\frac{d^2V_{dc}}{dt^2} > 0$. It is equivalent to $(A_1 - A_2) > 0$ in the first swing of current through dc link capacitor.

If the V_{dc} trajectory after fault clearance consists of low and high frequency components, signal decomposition techniques can be used to extract the different frequency components. The proposed criterion is then applied on the low frequency component of the V_{dc} trajectory as shown in Fig. 4(b). The high frequency components should be checked for positive damping to ensure stability of the system.

The dc link capacitor voltage can be monitored through a measuring device (a voltage sensor) at the dc link terminals (or dc bus) of PV generator. The first and second order derivatives of the capacitor voltage can be calculated using numerical differentiation methods viz., Newton's central difference,

Stiring's, Bessel's interpolation formulae [25]. In practical scenarios, the dc link voltage signal may have measurement noise. It is suggested that a filter should be used to remove the measurement noise from dc link voltage before applying the proposed criterion. The threshold parameters ϵ_1 and ϵ_2 can be considered in the proposed criterion to overcome the impact of measurement noise and numerical approximation on the stability assessment criterion.

- Stable scenario:

$$\left|\frac{dV_{dc}}{dt}\right| < \epsilon_1\Big|_{t=t^*} \;\&\; \frac{d^2V_{dc}}{dt^2} > \epsilon_2\Big|_{t=t^*} \;\&\; V_{dc}(t^*) \leq V_{dc_0}$$

- Unstable scenario:

$$\left|\frac{dV_{dc}}{dt}\right| < \epsilon_1\Big|_{t=t^*} \;\&\; \frac{d^2V_{dc}}{dt^2} > \epsilon_2\Big|_{t=t^*} \;\&\; V_{dc}(t^*) > V_{dc_0}$$

The parameters ϵ_1 and ϵ_2 should be chosen based on the expected measurement noise and numerical approximation.

D. IMPACT OF DC OVER-VOLTAGE PROTECTION ON PROPOSED CRITERION

During a Short Circuit (SC) fault, one of the following scenarios can occur depending on the dc link voltage overshoot:

- If the PV generator is required to have LVRT, the dc link capacitor voltage rating should be chosen so as to handle a predefined threshold value of V_{dc} overshoot. In addition, the pick up value of the dc over-voltage protection scheme should also be set accordingly. In this work, the PV generator is considered to possess LVRT capability. As a result, the dc link is designed considering a safety factor to satisfy the LVRT requirement.
- In an unforeseen scenario, if the dc link over-voltage exceeds the designed safety factor, the dc over-voltage protection scheme gets activated and disconnects the PV generator from the grid. The proposed method continues the online transient stability assessment till the PV generator gets disconnected. If PV generator becomes unstable before dc link capacitor protection gets activated, then the proposed method detects the unstable scenario.

The simulation results presented in the following section validate the transient stability assessment criterion.

IV. RESULTS

A. VALIDATION OF PROPOSED CRITERION ON SPIB SYSTEM

1) MODEL DESCRIPTION OF *SPIB* SYSTEM

The proposed criterion to assess the transient stability is implemented on the SPIB system presented in Fig. 1(b) and Fig. 2. The parameters of the SPIB system used in the present study are given in TABLE 1. The PI parameters presented in the TABLE 1 are designed so as to achieve fast and well damped response when subjected to a step change in V_{dc}^{ref} and Q_{ref} using Ziegler-Nicholas rule. The dc-ac converter of PV generator converts the dc voltage to 415 V, 60 Hz. Then the PV generator is connected to 11 kV, 60 Hz grid through a step up transformer. The PV generator is the clustered equivalent of 20 PV converter units with each of 100 kW rating. The configuration of the PV generator representing individual converter units can be found in [26]. The dc over-voltage protection scheme pick up value of each converter unit is chosen as 1.2 times the dc open circuit voltage [27]. So, the dc link protection scheme does not isolate the PV generator as along as $V_{dc} < 1.2 * V_{dc,oc}$, where $V_{dc,oc}$ denotes the PV array open circuit voltage. The PV equivalent model is obtained by accumulating the power and current rating of converters. However, the nominal voltage rating of equivalent model and the individual converter are equal. The present study is interested in system level dynamics instead of converter level dynamics. So, the configuration presented in Fig. 1(b) is considered to implement the proposed criterion. It is to be noted that, the current rating accumulation may lead to high overshoot in the dc link voltage during fault scenarios. As the dc over-voltage rating for each converter unit is 1.2 times the $V_{dc,oc}$, the dc over-voltage rating for the equivalent model (20 converters) is 5 times $V_{dc,oc}$. Further discussion on dc over-voltage of equivalent model is presented in section IV-A3.

TABLE 1. Parameters of The SPIB System.

Parameter	Value	Parameter	Value
V_{oc} (PV)	1.5 kV	I_{sc} (PV)	1.5 kA
S (rated)	2 MVA	P (output)	1.8 MW
L_f	0.5 mH	C_f	120 μF
G	1000 W/m^2	C	10000 μF
V_{dc}^{ref}	1.2 kV	Q_{ref}	0 $MVar$
X_L	3.77 Ω	Grid	11 kV, 60 Hz
$K_{p_{1,3}}$	0.5	$K_{i_{1,3}}$	10
$K_{p_{2,4}}$	5	$K_{i_{2,4}}$	200

For the proposed criterion, the stirling's formula is chosen for calculating the first and second derivatives of V_{dc}. The stirling's formula is chosen considering its accuracy and number of computations required as compared to other methods.

$$\begin{aligned}\frac{dV_{dc}}{dt}|_{t=t_1} &= \frac{1}{\Delta t}\Big(\frac{1}{2}(\delta^1 V_{dc,0} + \delta^1 V_{dc,-1}) \\ &\quad - \frac{1}{12}(\delta^3 V_{dc,-1} + \delta^3 V_{dc,-2}) \\ &\quad + \frac{1}{60}(\delta^5 V_{dc,-2} + \delta^5 V_{dc,-3})\Big) \\ \frac{d^2V_{dc}}{dt^2}|_{t=t_1} &= \frac{1}{\Delta t^2}\Big(\delta^2 V_{dc,-1} - \frac{1}{12}\delta^4 V_{dc,-2} + \frac{1}{90}\delta^6 V_{dc,-3}\Big)\end{aligned} \tag{10}$$

In (10), $\delta^i\ V_{dc,j}$ denotes the entries of difference table; δ^i represents the order of the difference column; j represents the index of the difference element in δ^{ith} column; Δt is the sampling time. As the first and second derivatives of V_{dc} are calculated using stirling's formula, the derivative of V_{dc} at t_1 is calculated after acquiring the samples till $t_1 + 4\ \Delta t$. Empirical Mode Decomposition (EMD) method [22] is used

here to decompose the V_{dc} trajectory into different components. The EMD method is widely used in the analysis of non-linear and non-stationary time series data. By using the EMD method, the V_{dc} trajectory can be separated into a set of high frequency components and a low frequency component (termed as residue in EMD method). To verify the functionality of the proposed criterion two different configurations of PV generator are considered here: i) Single stage configuration: PV arrays are connected to dc-ac converter which is then connected to the grid through a transformer. ii) Two stage configuration: PV arrays are connected to dc-dc converter for stepping up the dc voltage. The dc-dc converter is connected to a dc-ac converter which is then connected to the grid through a transformer.

2) SINGLE-STAGE PV GENERATOR CONFIGURATION

LLLG fault at PV end of the transmission line: A LLLG fault is created at PV end of the transmission line at $t = 5$ s. The stability of the system is assessed based on the criterion proposed in section III-B. The stability analysis is carried out using the proposed criterion by clearing the fault at different fault clearing times. It is observed that the SPIB system is stable when the fault clearing time is less than or equal to 187 ms. The system becomes unstable when fault is cleared after 188 ms of fault inception. The trajectories of V_{dc} for fault clearance times of 187 ms and 188 ms are presented in Fig. 7. From the Fig. 7 it can be seen that the V_{dc} trajectory has more than one frequency component. To assess the stability of the SPIB system EMD is employed to decompose the obtained V_{dc} trajectory. Fig. 7(a) and Fig. 7(b) present the different frequency components of the V_{dc} trajectory.

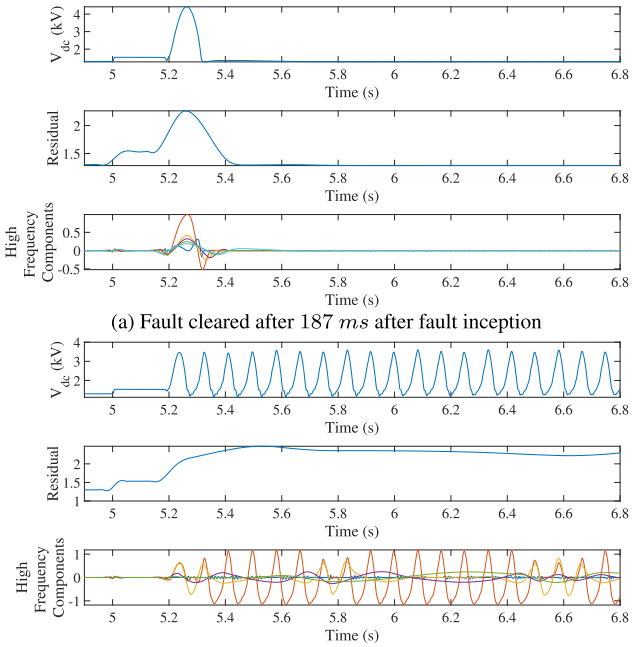

(a) Fault cleared after 187 ms after fault inception

(b) Fault cleared after 188 ms after fault inception

FIGURE 7. Empirical mode decomposition of V_{dc} trajectory.

In the figures, the low frequency component is denoted as residual component as termed in EMD and rest of the high frequency components are presented separately. It can be noticed from the residual component of Fig. 7(a), that $\frac{dV_{dc}}{dt} = 0$ & $\frac{d^2V_{dc}}{dt^2} > 0$ occur at $t = 5.5$ s and corresponding voltage is less than the pre-fault voltage. From Fig. 7(a) it can also be noticed that all the high frequency oscillations gets damped out around $t = 5.6$ s. However in the residual component of Fig. 7(b), $\frac{dV_{dc}}{dt} = 0$ & $\frac{d^2V_{dc}}{dt^2} > 0$ occurs at $t = 5.8$ s and corresponding voltage is greater than the pre-fault voltage. So, the proposed criterion declares the system to be unstable when fault is cleared after 188 ms of fault inception.

To validate the obtained result, the complete time-domain simulations i.e. till the system settles down, are performed for the SPIB system using PSCAD software. The results obtained from the simulations are presented in Fig. 8(a) - Fig. 8(h). From Fig. 8, it can be seen that the SPIB system is stable when fault is cleared at $t = 5.187$ s and system becomes unstable when fault is cleared at $t = 5.188$ s. In Fig. 8(a), 8(c), 8(e), 8(g) (i.e. fault clearance after 187 ms from fault inception), even though oscillations die out around 6 s the system has reached the stable operating point (operating equilibrium) at 13 s. This is due to the fact that the duty ratio of the PV converter switches has hit the maximum limit as shown in Fig. 8(e). The time taken for the the system to reach steady state is highly dependent on the

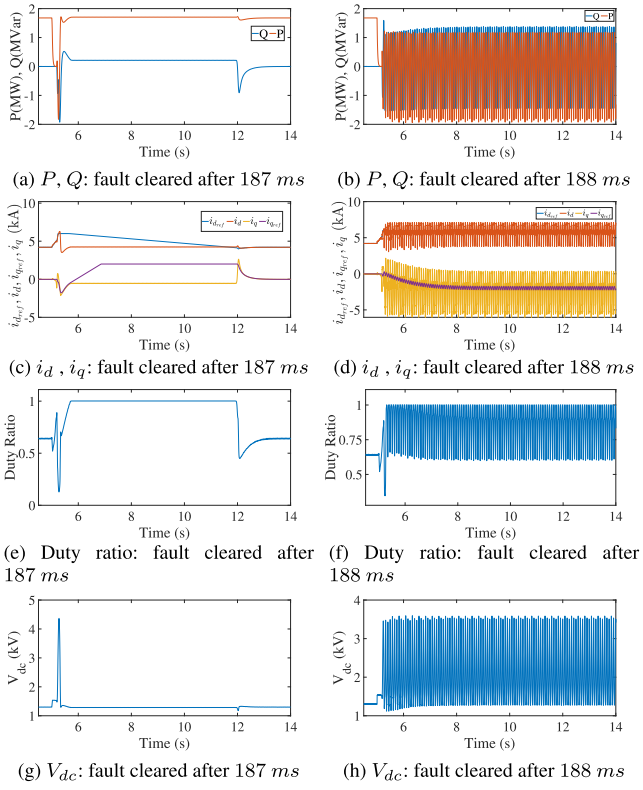

(a) P, Q: fault cleared after 187 ms

(b) P, Q: fault cleared after 188 ms

(c) i_d , i_q: fault cleared after 187 ms

(d) i_d , i_q: fault cleared after 188 ms

(e) Duty ratio: fault cleared after 187 ms

(f) Duty ratio: fault cleared after 188 ms

(g) V_{dc}: fault cleared after 187 ms

(h) V_{dc}: fault cleared after 188 ms

FIGURE 8. Time-domain simulation results:LLLG fault at PV end of the transmisssion line.

control parameters of the PV generator. On the other hand, the proposed criterion utilizes the V_{dc} trajectory only till $t = 5.6\ s$ in stable case and till $t = 5.85\ s$ in unstable case. So, the proposed criterion does not require the complete trajectory of the system i.e. till it reaches steady state. The time-domain simulation results shown in Fig. 8 validate the proposed criterion.

LLLG fault on the transmission line: A LLLG fault is created at $t = 5\ s$ on the middle of the transmission line connecting PV generator to the grid. The proposed criterion has identified that the system is stable if the fault is cleared before or at $t = 5.196\ ms$. When the fault is cleared at $t = 5.197\ ms$, the proposed stability criterion is not satisfied. The time-domain simulation results for fault duration of 196 *ms* and 197 *ms* are presented in Fig. 9.

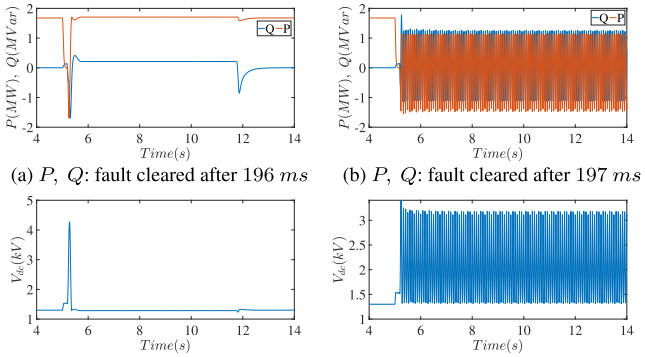

(a) $P,\ Q$: fault cleared after 196 ms (b) $P,\ Q$: fault cleared after 197 ms

(c) V_{dc}: fault cleared after 196 ms (d) V_{dc}: fault cleared after 197 ms

FIGURE 9. Time-domain simulation results: LLLG fault at midpoint of the line.

LLLG fault cleared by switching out the faulty parallel line: A LLLG fault is created at $t = 5\ s$ at the PV end of one of the parallel transmission lines connecting PV generator to the grid. The fault is cleared by switching out the faulty parallel transmission line. The proposed criterion has identified that the system is stable if the fault is cleared before or at $t = 5.222\ ms$. When the fault is cleared at $t = 5.223\ ms$, the proposed stability criterion is not satisfied. The time-domain simulation results for fault duration of 222 *ms* and 223 *ms* are presented in Fig. 10.

LLLG fault with fault resistance: A LLLG fault with fault resistance of 2 Ω is created at $t = 5\ s$ at the PV end of the transmission line connecting PV generator to the grid. The proposed criterion has identified that the system is stable if the fault is cleared before or at $t = 5.508\ ms$. When the fault is cleared at $t = 5.509\ ms$, the proposed stability criterion is not satisfied. The simulation results for fault duration of 508 *ms* and 509 *ms* are presented in Fig. 11.

The results presented in the Fig. 9, Fig. 10 and Fig. 11 validate the effectiveness of the proposed criterion in determining the system stability. It is to be noted that in Fig. 9, Fig. 10 and Fig. 11 the system has become unstable before the dc link over-voltage protection is activated.

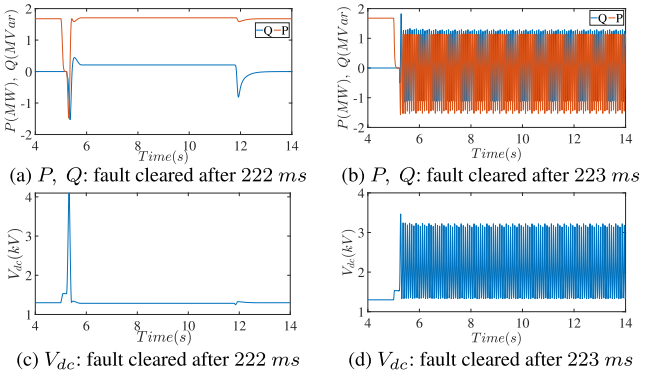

(a) $P,\ Q$: fault cleared after 222 ms (b) $P,\ Q$: fault cleared after 223 ms

(c) V_{dc}: fault cleared after 222 ms (d) V_{dc}: fault cleared after 223 ms

FIGURE 10. Time-domain simulation results: LLLG fault cleared by switching out the faulty parallel line.

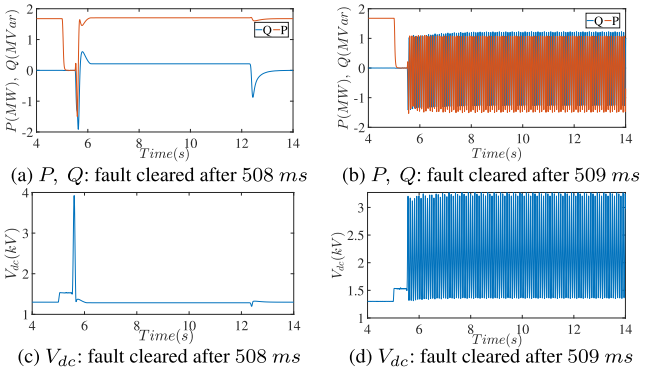

(a) $P,\ Q$: fault cleared after 508 ms (b) $P,\ Q$: fault cleared after 509 ms

(c) V_{dc}: fault cleared after 508 ms (d) V_{dc}: fault cleared after 509 ms

FIGURE 11. Time-domain simulation results: LLLG fault with fault resistance.

3) DC LINK DYNAMICS

It can be seen in Fig. 8 - Fig. 11 the maximum transient value of V_{dc} after clearing the fault (i.e. $t = 5.2\ s$ to $t = 5.3\ s$) is obtained as $4.3\ kV$. The peak value is around 3 times the Open Circuit (OC) voltage $1.5\ kV$. To understand the reason behind the over-voltage in V_{dc}, the dynamics of dc link capacitor (when SPIB system is subjected to LLLG fault for 187 *ms*) is investigated here. From Fig. 12(a) and Fig. 12(b) it can be seen that during the time interval of $t = 5.2\ s$ to $t = 5.3\ s$,

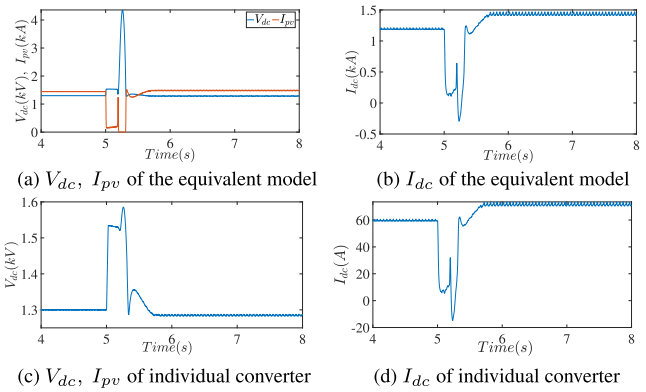

(a) $V_{dc},\ I_{pv}$ of the equivalent model (b) I_{dc} of the equivalent model

(c) $V_{dc},\ I_{pv}$ of individual converter (d) I_{dc} of individual converter

FIGURE 12. DC link dynamics: LLLG fault.

the I_{pv} is zero and I_{dc} is negative. I_{pv} denotes the output current of PV array and I_{dc} represents the input current to the PV converter as shown in Fig. 1(b). So from Fig. 12(a) and Fig. 12(b), it can be concluded that I_{dc} (i.e. current flowing into the dc link capacitor) is responsible for the over-voltage in V_{dc}. As mentioned in section IV-A1, the equivalent model of PV generator is built by accumulating the current rating of 20 converter units. So, in the full model of PV generator, I_{dc} (i.e. current responsible for charge accumulation) will be divided among the 20 parallel converter units. The I_{dc} value flowing in to each of the parallel converter units is presented in Fig. 12(d). The V_{dc} trajectory corresponding to I_{dc} in Fig. 12(d) is presented in Fig. 12(c). It can be seen that the maximum value of the transient voltage is 1.58 kV (i.e. 1.05 times the OC value). The PV converters are rated to withstand dc over-voltages up to 1.2 times the dc open circuit voltage [27]. So, the dc link voltage is within the over-voltage rating of the PV converter. It is to be noted that, the dissimilarity in V_{dc} transients between the equivalent model and individual converter model does not affect the effectiveness of the stability criterion. This is due to the fact that the proposed criterion is based on net charge accumulation of dc link capacitor after fault rather than the absolute charge accumulation.

To understand the impact of type of the disturbance on dc link over-voltage, the dc link voltage dynamics are investigated here considering different types of disturbances on the SPIB system. Out of the numerous investigated scenarios, the dynamics of V_{dc} for: (i) LLLG fault at PV end of transmission line for 100 *ms*, (ii) LLG fault at PV end of transmission line for 500 *ms*, (iii) Step change in V_{dc}^{ref}, (iv) DC side short-circuit fault in one of the PV array strings are presented here. The disturbances are chosen so as to investigate the dc link dynamics when disturbances with different severity and duration of disturbance are considered. The dc link voltage trajectories under the chosen disturbances are shown in Fig. 13. The V_{dc} trajectories presented in Fig. 13 correspond to the equivalent model of PV generator. From Fig. 8 and Fig. 13 it is to be noted that for LLLG fault at PV end, when the fault duration is decreased from 187 *ms* to 100 *ms* there is huge decrease in the transient dc link voltage.

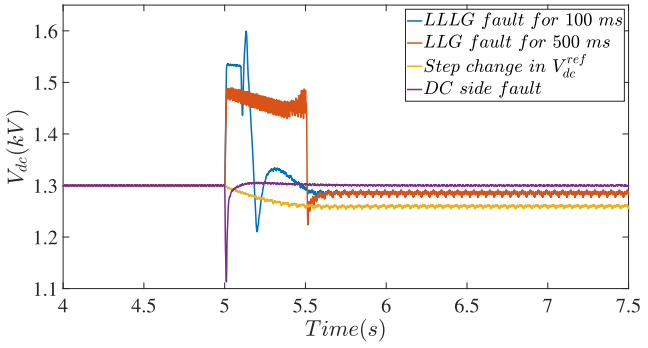

FIGURE 13. Dynamics of V_{dc}: different types of disturbances.

It can be seen that the dc link voltage transients are within the over-voltage limit of the PV converters. From the obtained results, it is identified that the transients in dc link voltage are mainly due to the error accumulation in the PI blocks of current control. From the carried out studies, it is concluded that the severity and duration of the disturbances are the factors that determine the magnitude of transient voltage of the dc link capacitor.

4) CRITICAL CLEARING TIME CALCULATION

In section IV-A2 and section IV-A3, the transient stability of SPIB system is investigated considering different types of disturbances. From the studies presented in section IV-A2 and section IV-A3, the Critical Clearing Time (CCT) is obtained as 187 *ms* by the proposed stability criterion. The time-domain simulation results presented in Fig. 8- Fig. 11 and Fig. 13 show that the CCT of SPIB system is equal to 187 *ms*. So, the CCT obtained from time-domain simulations match with the value obtained from proposed criterion.

As the proposed criterion is developed based on the energy stored in the dc link capacitor, the criterion can be employed for two stage converter configuration of PV generator system. The criterion is investigated for a two stage PV generator in the following section.

5) TWO-STAGE PV GENERATOR CONFIGURATION

The two-stage configuration of the PV generator system is employed from [28]. The two-stage PV generator comprises of a dc-dc boost conversion stage and a dc-ac conversion stage. The parameters of the two-stage PV generator are presented in TABLE 2. In TABLE 2, L_{dc} and C_{dc} denote the inductance and capacitance of the dc-dc boost converter of the PV generator; C_{pv} denotes the capacitance at the terminals of the PV array. The C_{dc} acts as the dc link capacitance which is connected between the dc-dc converter and dc-ac converter. The steady state operating point of the system is considered to be same as that of the single stage PV generator discussed in section IV-A1. The results obtained from the proposed criterion and the time-domain simulations are presented here. A LLLG fault is considered at the PV end of the transmission line, fault occurrence instant is considered

TABLE 2. Parameters of the SPIB System (Two Stage Configuration).

Parameter	Value	Parameter	Value
V_{oc} (PV)	0.5 kV	I_{sc} (PV)	5 kA
S (rated)	2 MVA	P (output)	1.8 MW
L_f	0.5 mH	C_f	120 μF
G	1000 W/m^2	C_{pv}	1000 μF
L_{dc}	1 mH	C_{dc}	10000 μF
V_{dc}^{ref}	1.2 kV	Q_{ref}	0 $MVar$
X_L	3.77 Ω	Grid	11 kV, 60 Hz
$K_{p_{1,3}}$	1.5	$K_{i_{1,3}}$	10
$K_{p_{2,4}}$	8.2	$K_{i_{2,4}}$	500

at $t = 5\ s$. The EMD of the dc link capacitance voltage for stable and unstable cases are shown in Fig. 14 (a) and Fig. 14 (b). The proposed criterion assesses the system to be stable for fault clearance at $t = 5.122\ s$ and system to be unstable for fault clearance instant at $t = 5.123\ s$. The corresponding time-domain results obtained using PSCAD software are presented in Fig. 15. The results presented in Fig. 15 validate the proposed criterion.

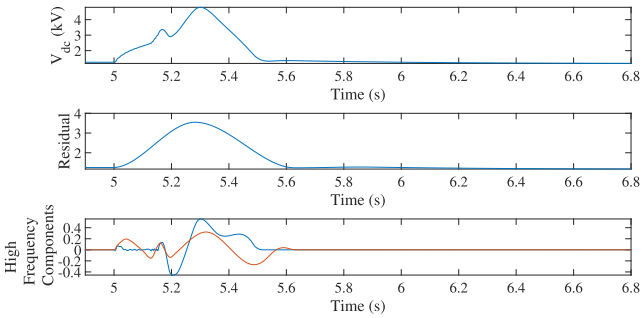

(a) Fault cleared after 122 ms after fault inception

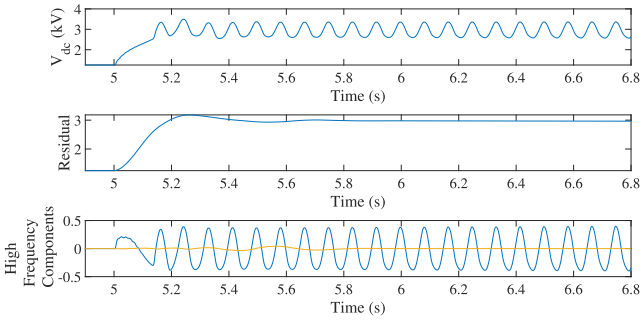

(b) Fault cleared after 123 ms after fault inception

FIGURE 14. Empirical mode decomposition of V_{dc} trajectory.

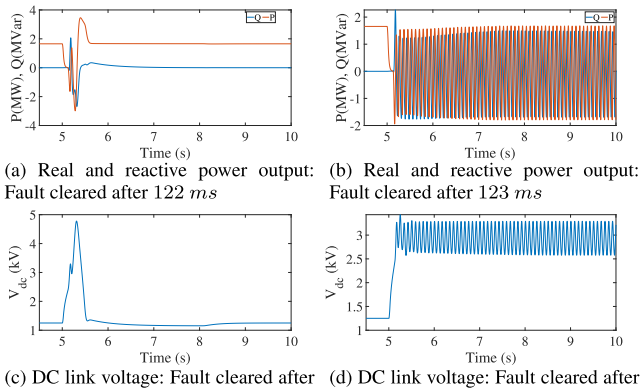

(a) Real and reactive power output: Fault cleared after 122 ms

(b) Real and reactive power output: Fault cleared after 123 ms

(c) DC link voltage: Fault cleared after 122 ms

(d) DC link voltage: Fault cleared after 123 ms

FIGURE 15. Time-domain simulation results.

B. VALIDATION OF PROPOSED CRITERION ON MULTI-MACHINE SYSTEM

To validate the functionality of the proposed criterion on multi-machine power systems, the IEEE-39 bus system is considered. In order to carry out transient stability analysis of grid-connected PV, the benchmark system is modified by adding a PV generator. A PV generator is added to the system through a transformer and a transmission line connected at bus no. 9 as shown in Fig. 16. The parameters of the PV generator and the transformer are same as that of presented in TABLE 1 except for V_{dc}^{ref} which is equal to 1.35 kV. The transmission line connecting bus no. 40 and bus no. 9 is 80 km long with an impedance of 0.37 Ω/km.

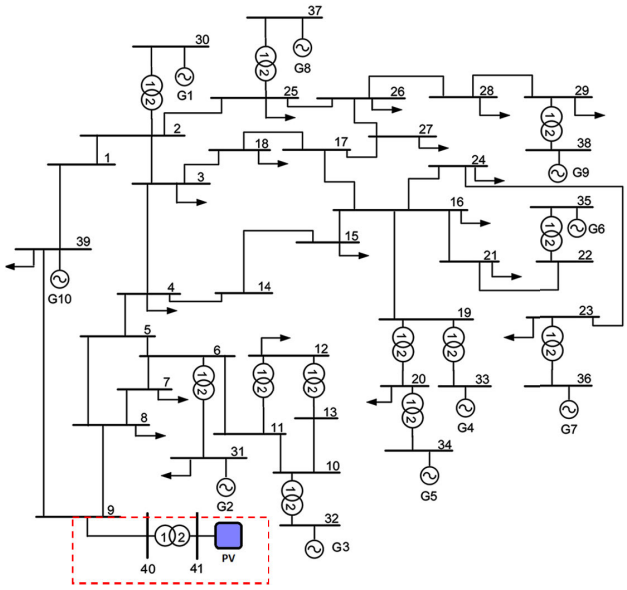

FIGURE 16. Modified IEEE-39 bus system with a PV generator.

1) FAULT ON BUS NO. 40

A LLLG fault is considered on bus no. 40 of the modified IEEE 39 bus system. The fault is created at $t = 10\ s$. From the proposed criterion for transient stability, it is observed that the system is transient stable when fault is created before or at $t = 10.287\ s$. The corresponding time-domain results are presented in Fig. 17. The trajectories presented in Fig. 17 show that system is stable when fault is cleared after 287 ms of fault inception and system is unstable when fault is cleared after 288 ms of fault inception. The obtained time-domain results validate the proposed criterion.

2) FAULT ON THE TRANSMISSION LINE CONNECTING BUS NO. 40 AND BUS NO. 9

A LLLG fault is considered on the middle point of transmission line connecting bus no. 40 and bus no. 9 of the modified IEEE 39 bus system. The fault is created at $t = 10\ s$. The system is found to be transient stable if fault is created before or at $t = 10.294\ s$ by employing the proposed criterion. The time-domain results for fault cleared at $t = 10.294\ s$ and $t = 10.295\ s$ are presented in Fig. 18. The Fig. 18 shows that system is stable when fault is cleared after 294 ms of fault inception and system is unstable when fault is cleared after 295 ms of fault inception. So, the time-domain results validate the proposed criterion.

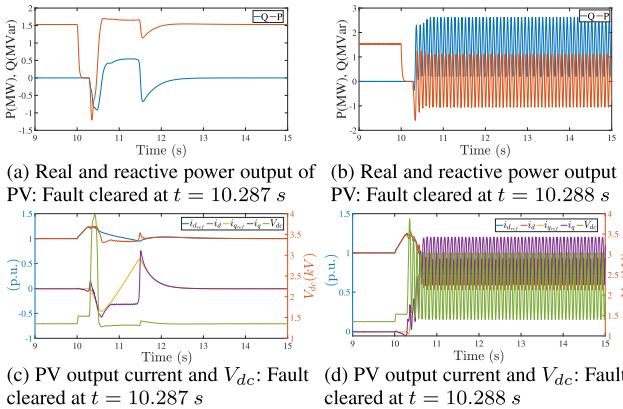

(a) Real and reactive power output of PV: Fault cleared at $t = 10.287\ s$

(b) Real and reactive power output of PV: Fault cleared at $t = 10.288\ s$

(c) PV output current and V_{dc}: Fault cleared at $t = 10.287\ s$

(d) PV output current and V_{dc}: Fault cleared at $t = 10.288\ s$

FIGURE 17. Time-domain simulation results.

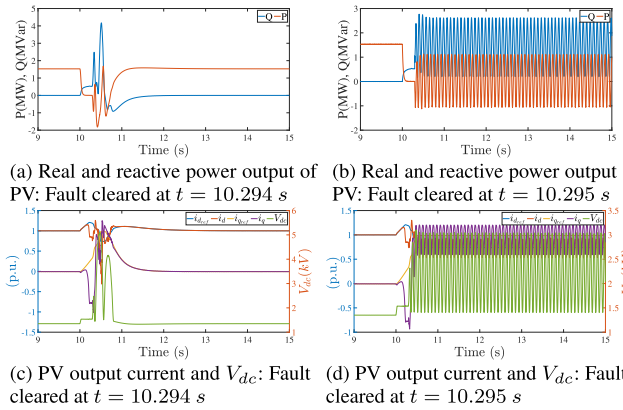

(a) Real and reactive power output of PV: Fault cleared at $t = 10.294\ s$

(b) Real and reactive power output of PV: Fault cleared at $t = 10.295\ s$

(c) PV output current and V_{dc}: Fault cleared at $t = 10.294\ s$

(d) PV output current and V_{dc}: Fault cleared at $t = 10.295\ s$

FIGURE 18. Time-domain simulation results.

C. COMPARISON OF THE PROPOSED CRITERION WITH AN EXISTING TRANSIENT STABILITY CRITERIA FOR V_{dc} AND Q CONTROL BASED PV

In this section the proposed criterion is compared with stability criterion available in existing literature. In the existing literature, there are works reported on transient stability assessment criterion for grid connected VSCs equipped with power synchronization control and droop control [3], [4], [6], [8], [12], [13]. However, transient stability assessment of V_{dc} and Q control based PV generation is reported only in [14]. The transient stability criterion presented in [14] is chosen for comparison because the methods presented in [3], [4], [6], [8], [12], [13] are not applicable for V_{dc} and Q control based PV generator.

In [14], the stability is assessed by examining voltage recovery and area under the curves $f_1(x)$ *vs.* d_d and $f_2(x)$ *vs.* d_q. The non-linear functions $f_1(x)$ and $f_2(x)$ are given by:

$$\begin{aligned} f_1(x) &= K_{i_2}K_{p_1}\frac{d(V_{dc}-V_{dc}^{ref})}{dt} - K_{i_2}\frac{di_d}{dt} \\ &\quad + K_{i_2}K_{i_1}(V_{dc}-V_{dc}^{ref}) \\ f_2(x) &= K_{i_4}K_{p_3}\frac{d(Q-Q_{ref})}{dt} - K_{i_4}\frac{di_q}{dt} \\ &\quad + K_{i_4}K_{i_3}(Q-Q_{ref}) \end{aligned} \tag{11}$$

The comparison of the proposed criterion with the criterion presented in [14] is discussed in the following sections. The SPIB system with single-stage PV generator configuration is considered here for the comparison.

1) AMOUNT OF DATA PROCESSED

The criterion in [14] requires monitoring of V_{dc}, V_{pv}, i_d, i_q, d_d and d_q. The proposed criterion in this work requires monitoring of V_{dc} alone. This leads to the advantage of reduced signal handling and less prone to measurement error compared to the criterion in [14]. The amount of data to be processed by the criteria for four different fault scenarios (on the transmission line) is presented in TABLE 3. The TABLE 3 represents the amount of data to be processed by the criteria in equal time duration. The TABLE 3 highlights the reduction in amount of data to be processed for the proposed criterion as compared to the criterion in [14].

TABLE 3. Comparison of amount of data to be processed by the criteria.

Type of fault (fault duration)	Data size	
	proposed criterion	criterion [14]
LLLG fault at PV end (150 ms)	34.9 kB	209.8 kB
LLLG fault at mid-point (200 ms)	36.4 kB	218.9 kB
LLG fault at PV end (150 ms)	34.9 kB	209.8 kB
LLG fault at mid-point (200 ms)	36.4 kB	218.9 kB

2) COMPUTATION TIME

To implement the criterion in [14] the non-linear functions should be calculated which in-turn requires the computation of derivatives shown in (11). After computing the values on the nonlinear functions, area under the curves $f_1(x)$ *vs.* d_d and $f_2(x)$ *vs.* d_q should be calculated for stability assessment. On the other hand, the proposed criterion in this work is based on investigation of capacitor voltage. To compare the computational requirement of the criteria, *timeit* function of MATLAB is used. As the computation time taken for implementing the criteria is dependent on type of the processor used, ratio of computation times is presented here through parameter γ_{comp}. The γ_{comp} is defined as:

$$\gamma_{comp} = \frac{\text{Computation time for criterion in [14]}}{\text{Computation time for the proposed criterion}}$$

The ratio of computation times taken by the criteria for stability assessment for four different fault scenarios is presented in TABLE 4. From TABLE 4 it can be seen that the proposed criterion can assess the stability much faster than the criterion in [14]. This points out the advantage of computational requirement of the proposed criterion over the criterion in [14].

TABLE 4. Comparison of computation time.

Type of fault (Fault duration)	Ratio of stability estimation time (γ_{comp})
LLLG fault at PV end (150 ms)	11.84
LLLG fault at mid-point (200 ms)	12.4
LLG fault at PV end (150 ms)	11.95
LLG fault at mid-point (200 ms)	12.15

3) ACCURACY

The accuracy of the criteria is compared here by computing CCT of the system. The CCT calculation is chosen because it involves investigation of numerous disturbances like LLLG fault, LLG fault, faults followed by loss of transmission line. When the CCT is calculated by employing the criterion in [14], the CCT is obtained as 187 *ms*. In section IV-A4 it is identified that the CCT obtained from proposed criterion is also 187 *ms* which is inline with the time domain simulations. So, the CCT obtained from the proposed criterion and the criterion in [14] are equal.

In summary, the above discussion marks that the proposed criterion has advantage in amount of data to be handled, number of computations required to implement the criterion and is less prone to measurement error compared to the approach in [14]. However, the accuracy of the proposed criterion and the criterion in [14] is equal.

V. CONCLUSION

An online transient stability assessment criterion for grid connected PV generator (V_{dc} and Q control) is proposed in this paper. The PV generator in the study is equipped with LVRT capability. The stability of grid connected PV generator is assessed based on the net energy of the dc link capacitor after the first swing of the capacitor voltage. Time-domain simulations are carried out to validate the effectiveness of the proposed criterion on SPIB and a modified IEEE-39 bus system. The proposed method is validated on two different types of PV configurations viz., single stage and two stage converter. From the studies carried out, it is identified that the proposed criterion can accurately estimate the critical clearing time. The dc link voltage dynamics are also presented considering various types of system disturbances (symmetrical and asymmetrical faults, dc side fault, change in reference values of the PV control) with different severity levels and duration of disturbance. From the studies, it is observed that the dc link voltage overshoot depends on the severity and duration of disturbance on the system. In the investigated scenarios, the system has become unstable even before the dc link over-voltage limit is hit. The proposed criterion is compared against an existing transient stability criterion considering the aspects of amount of data required, computation time and accuracy of the criteria. The proposed criterion is found to be computationally efficient and it requires lesser measurements compared to the existing technique while maintaining the same accuracy.

REFERENCES

[1] P. Kundur, N. J. Balu, and M. G. Lauby, *Power System Stability and Control*, vol. 7. New York, NY, USA: McGraw-Hill, 1994.
[2] N. Hatziargyriou, J. Milanović, C. Rahmann, V. Ajjarapu, C. Cañizares, I. Erlich, D. Hill, I. Hiskens, I. Kamwa, B. Pal, and P. Pourbeik, "Stability definitions and characterization of dynamic behavior in systems with high penetration of power electronic interfaced technologies," in *Proc. IEEE PES*, Apr. 2020, pp. 1–42.
[3] H. Wu and X. Wang, "Design-oriented transient stability analysis of grid-connected converters with power synchronization control," *IEEE Trans. Ind. Electron.*, vol. 66, no. 8, pp. 6473–6482, Aug. 2019.
[4] M. Li, W. Huang, N. Tai, and M. Yu, "Lyapunov-based large signal stability assessment for VSG controlled inverter-interfaced distributed generators," *Energies*, vol. 11, no. 9, p. 2273, Aug. 2018.
[5] I. R. S. Priyamvada and S. Das, "Transient stability analysis of VSC based photo-voltaic generator with PQ control connected to infinite bus," in *Proc. IEEE Power Energy Soc. Gen. Meeting (PESGM)*, Aug. 2019, pp. 1–5.
[6] M. Li, W. Huang, N. Tai, M. Yu, Y. Lu, and C. Ni, "Transient behavior analysis of VSG-IIDG during disturbances considering the current limit unit," in *Proc. IEEE Power Energy Soc. Gen. Meeting (PESGM)*, Aug. 2019, pp. 1–5.
[7] I. R. S. Priyamvada and S. Das, "Critical clearing time calculation using energy functions for VSC based grid connected PV generators with PQ control," in *Proc. IEEE Milan PowerTech*, Jun. 2019, pp. 1–6.
[8] X. He, H. Geng, and S. May, "Transient stability analysis of grid-tied converters considering PLL's nonlinearity," *CPSS Trans. Power Electron. Appl.*, vol. 4, no. 1, pp. 40–49, Mar. 2019.
[9] X. He, H. Geng, R. Li, and B. C. Pal, "Transient stability analysis and enhancement of renewable energy conversion system during LVRT," *IEEE Trans. Sustain. Energy*, vol. 11, no. 3, pp. 1612–1623, Jul. 2020.
[10] X. He, H. Geng, J. Xi, and J. M. Guerrero, "Resynchronization analysis and improvement of grid-connected VSCs during grid faults," *IEEE J. Emerg. Sel. Topics Power Electron.*, early access, Nov. 20, 2019, doi: 10.1109/JESTPE.2019.2954555.
[11] Q. Hu, L. Fu, F. Ma, and F. Ji, "Large signal synchronizing instability of PLL-based VSC connected to weak AC grid," *IEEE Trans. Power Syst.*, vol. 34, no. 4, pp. 3220–3229, Jul. 2019.
[12] D. Pan, X. Wang, F. Liu, and R. Shi, "Transient stability of voltage-source converters with grid-forming control: A design-oriented study," *IEEE J. Emerg. Sel. Topics Power Electron.*, vol. 8, no. 2, pp. 1019–1033, Jun. 2020.
[13] L. Huang, H. Xin, Z. Wang, L. Zhang, K. Wu, and J. Hu, "Transient stability analysis and control design of droop-controlled voltage source converters considering current limitation," *IEEE Trans. Smart Grid*, vol. 10, no. 1, pp. 578–591, Jan. 2019.
[14] I. R. S. Priyamvada and S. Das, "Transient stability of V_{dc}—Q control-based PV generator with voltage support connected to grid modelled as synchronous machine," *IEEE Access*, vol. 8, pp. 130354–130366, 2020.
[15] S. Mortazavian and Y. A.-R.-I. Mohamed, "Investigation and enhancement of stability in grid-connected converter-based distributed generation units with dynamic loads," *IEEE Access*, vol. 8, pp. 93426–93443, 2020.
[16] Y. Ren, R. Duan, L. Chen, W. Huang, C. Wu, and Y. Min, "Stability assessment of grid-connected converter system based on impedance model and gershgorin theorem," *IEEE Trans. Energy Convers.*, vol. 35, no. 3, pp. 1559–1566, Sep. 2020.
[17] W. Wei, Y. Xia, and F. Blaabjerg, "Nonlinear stability analysis for three-phase grid-connected PV generators," *IEEE J. Emerg. Sel. Topics Power Electron.*, vol. 8, no. 4, pp. 3487–3501, Dec. 2020.
[18] F. Blaabjerg, R. Teodorescu, M. Liserre, and A. V. Timbus, "Overview of control and grid synchronization for distributed power generation systems," *IEEE Trans. Ind. Electron.*, vol. 53, no. 5, pp. 1398–1409, Oct. 2006.
[19] A. Yazdani and R. Iravani, *Voltage-Sourced Converters in Power Systems*, vol. 34. Hoboken, NJ, USA: Wiley, 2010.
[20] P. Kundur, J. Paserba, V. Ajjarapu, G. Andersson, A. Bose, C. Canizares, N. Hatziargyriou, D. Hill, A. Stankovic, C. Taylor, T. Van Cutsem, and V. Vittal, "Definition and classification of power system stability IEEE/CIGRE joint task force on stability terms and definitions," *IEEE Trans. Power Syst.*, vol. 19, no. 3, pp. 1387–1401, Aug. 2004.

[21] R. Teodorescu, M. Liserre, and P. Rodriguez, *Grid Converters for Photovoltaic and Wind Power Systems*, vol. 29. Hoboken, NJ, USA: Wiley, 2011.
[22] N. E. Huang, Z. Shen, S. R. Long, M. C. Wu, H. H. Shih, Q. Zheng, N.-C. Yen, C. C. Tung, and H. H. Liu, "The empirical mode decomposition and the Hilbert spectrum for nonlinear and non-stationary time series analysis," *Proc. Roy. Soc. London A, Math., Phys. Eng. Sci.*, vol. 454, no. 1971, pp. 903–995, Mar. 1998.
[23] R. Fontugne, P. Borgnat, and P. Flandrin, "Online empirical mode decomposition," in *Proc. IEEE Int. Conf. Acoust., Speech Signal Process. (ICASSP)*, Mar. 2017, pp. 4306–4310.
[24] H. Zhang, C. W. Rowley, E. A. Deem, and L. N. Cattafesta, "Online dynamic mode decomposition for time-varying systems," *SIAM J. Appl. Dyn. Syst.*, vol. 18, no. 3, pp. 1586–1609, Jan. 2019.
[25] B. Grewal, *Higher Engineering Mathematics*. New Delhi, India: Khanna Publishers, 2002.
[26] H. Wu, J. Zhang, C. Luo, and B. Xu, "Equivalent modeling of photovoltaic power station based on canopy-FCM clustering algorithm," *IEEE Access*, vol. 7, pp. 102911–102920, 2019.
[27] *ABB Central Inverters PVS800 100 to 500 kW*. Accessed: Oct. 20, 2020. [Online]. Available: http://new.abb.com/docs/librariesprovider22/technical-documentation/pvs800-central-inverters-flyer.pdf?sfvrsn=2
[28] M. Mirhosseini, J. Pou, and V. G. Agelidis, "Single- and two-stage inverter-based grid-connected photovoltaic power plants with ride-through capability under grid faults," *IEEE Trans. Sustain. Energy*, vol. 6, no. 3, pp. 1150–1159, Jul. 2015.

INDLA RAJITHA SAI PRIYAMVADA (Graduate Student Member, IEEE) received the B.Tech. degree in electrical engineering from the National Institute of Technology Calicut, India, in 2015. She is currently pursuing Ph.D. degree with the Department of Electrical Engineering, Indian Institute of Science, Bengaluru, India.

SARASIJ DAS (Senior Member, IEEE) received the Ph.D. degree from the University of Western Ontario, London, ON, Canada, in 2014. He was with the Global Technology Centre, Schneider Electric India Pvt., Ltd., Bengaluru, India, and Power Research and Development Consultants Pvt., Ltd., Bengaluru, India. He is currently an Assistant Professor with the Department of Electrical Engineering, Indian Institute of Science, Bengaluru, India.